# Supplementary Information

# Uncompromised Reinforcement: Polysiloxane with 100% Room-Temperature Self-Healing and Antifouling

Haoran Li[a, b], Yuheng Chen[a, c], Yanchao Wu[b, d], Huimin Qi[a, c]*, Huijing Li[b, d]*, Ga Zhang[a, c]*

*a. Key Laboratory of Science and Technology on Wear and Protection of Materials, Lanzhou Institute of Chemical Physics, Chinese Academy of Sciences, Lanzhou 730000, China*

*b. School of Chemistry and Chemical Engineering, Harbin Institute of Technology, Harbin 150006, China*

*c. Qingdao Center of Resource Chemistry & New Materials, Qingdao 266071 China*

*d. Weihai Key Laboratory of Active Factor of Marine Products, Weihai Marine Organism & Medical Technology Research Institute, Harbin Institute of Technology, Weihai 264209, China*

*Corresponding authors: Huimin Qi: qihuimin@licp.cas.cn, Huijing Li: lihj@hit.edu.cn, Ga Zhang: gzhang@licp.cas.cn

## Materials

3-(2-Aminoethylamino)propyltriethoxysilane, (3-aminopropyl)triethoxysilane, 3-aminopropyl(diethoxy)methylsilane, p-phthalaldehyde, silver nitrate and trimesic acid ($H_3BTC$) were purchased from Aladdin Industrial Corporation with analytical purity. Graphene oxide (GO) was purchased from Suzhou Tanfeng Graphene Technology Co., Ltd. *Pseudomonas* sp. and *Pseudoalteromonas* sp. were purchased from Ningbo Mingzhou Biotechnology Co., Ltd. Commercial concentrated *Chlorella* suspension was purchased from Yancheng Bainuo Biotechnology Co., Ltd.

## Characterizations

The thermal stability of the resins and fillers was characterized by thermogravimetric analysis (TG, TA Q500 instrument, USA). To characterize the tensile strength and self-healing behavior, tensile stress-strain curves were measured using a universal mechanical testing machine (Shimadzu AGS-X-50N, Japan) with a tensile rate of 5

mm/min. The self-healing performance was evaluated by tensile testing of fractured-and-reconnected samples at 25 ℃ and 37 ℃, with stress-strain curves quantifying the self-healing efficiency. The self-healing efficiency is defined as the percentage of the tensile strength after self-healing to that before self-healing. Rheological tests were performed using a TA DHR-2 rheometer (USA) with a stress of 2 kPa. The structural analysis of polysiloxane and Ag-BTC was carried out using X-ray diffraction (XRD, Rigaku SmartLab SE, Japan). The glass transition temperature (Tg) of polysiloxane was determined by differential scanning calorimetry (DSC, Netzsch DSC 200 F3, Germany). The sample surface morphology was examined by field emission scanning electron microscopy (SEM, Thermo Scientific Quattro S, USA). The chemical structural evolution during polysiloxane self-healing was characterized by Fourier-transform infrared spectroscopy (FTIR, Bruker TENSOR27, Germany). The optical density ($OD_{600}$ and $OD_{680}$) of bacterial and *Chlorella* suspensions was measured using a UV-Vis spectrophotometer (Beijing Purkinje, TU-1810DSPC, China). The $Ag^{+}$ concentration was determined using an inductively coupled plasma mass spectrometer (ICP, Agilent ICP-MS 7800, USA). The water contact angle (WCA) measurement was performed using a contact angle system (OCA20, China).

**Calculation Process of Apparent Activation Energy and Contribution Splitting of Dynamic Bonds**

The Arrhenius equation describes the relationship between the reaction rate constant (k) and temperature (T), which is expressed as:

$$lnk = -\frac{E_a}{R} \cdot \frac{1}{T} + lnA$$

Wherein:

$k$: Rate constant of the self-healing process ($s^{-1}$);

$E_a$: Apparent activation energy ($kJ \cdot mol^{-1}$);

$R$: Gas constant, $R = 0.008314\ kJ \cdot mol^{-1} \cdot K^{-1}$;

$T$: Absolute temperature ($K$), $T = t(℃) + 273.15$;

$A$: Pre-exponential factor (frequency factor) ($s^{-1}$).

The self-healing rate constants ($k$) at different temperatures were obtained from the self-healing efficiency (η, t=900 s) tests using a tensile testing machine.

$$k = \frac{1}{t} \ln\left(\frac{1}{1-\eta}\right)$$

The original experimental data and the arranged data for Arrhenius fitting are listed in Tab. S4.

The formula for calculating the contribution ratios of hydrogen bonds and dynamic covalent bonds during the self-healing process is as follows:

$$E_{a,\text{total}} = x \cdot E_{a,\text{H}} + (1 - x) \cdot E_{a,\text{imine}}$$

Wherein:

$E_{a,total}$ = measured total activation energy, 42.8 kJ·mol$^{-1}$

$E_{a,H}$ = activation energy of pure hydrogen bonding (typical value: 25 kJ·mol$^{-1}$)

$E_{a,imine}$ = activation energy of imine bond exchange (45 kJ·mol$^{-1}$ is used due to the relatively low self-healing temperature)

$x$ = contribution ratio of H-bond

$1-x$ = contribution ratio of imine bond

**Antifouling Test**

SDC, SDC-G, and SDC-GM coated samples were immersed in *Pseudomonas* sp. ($OD_{600}$ = 0.3) and *Pseudoalteromonas* sp. ($OD_{600}$ = 0.5) suspensions at 35 ℃ for 30 h, and in *Chlorella* ($OD_{680}$ = 0.5) suspension at 25 ℃ for 30 h, followed by WCA and SEM evaluation of microbial adhesion on the sample surfaces.

Tab. S1 Raw materials and their formulations for SDC and its composites.

| | 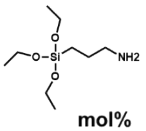 mol% | 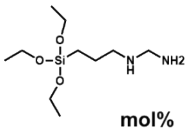 mol% | 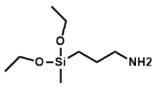 mol% | 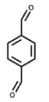 mol% | s-GO wt% | Ag-BTC wt% |
|---|---|---|---|---|---|---|
| **SDC** | 10.4 | 52.0 | 31.1 | 6.5 | — | — |
| **SDC-G** | 10.4 | 52.0 | 31.1 | 6.5 | 0.37 | — |
| **SDC-M** | 10.4 | 52.0 | 31.1 | 6.5 | — | 0.5 |
| **SDC-GM** | 10.4 | 52.0 | 31.1 | 6.5 | 0.37 | 0.5 |

Tab. S2 Raw materials and their formulations for SHS. The values in the table represent mol%.

| | 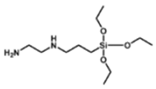 | 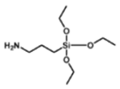 | 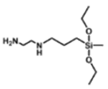 |  |  |
|---|---|---|---|---|---|
| **SHS-1** | 9 | 5 | 0.5 | 2 | 0.1 |
| **SHS-2** | 7 | 7 | 0.5 | 2 | 0.1 |
| **SHS-3** | 6 | 6 | 1 | 4 | 0.05 |

Tab. S3 Comparison of self-healing and antifouling properties between this work and other self-healing silicone antifouling materials

| Reference | Self-healing Efficiency | Antifouling Test Conditions | Antibacterial Rate/ Antifouling Performance |
|---|---|---|---|
| **This work** | 100% | Bacterial and *Chlorella* suspension, 30 h | 100% |
| Ref44 | 80.2% | Bacterial suspension, light exposure for 54 h | 100% |
| Ref 45 | Scratch healing | *C. vulgaris* suspension, 36 h | Rare fouling |
| Ref 46 | 98.95% | Bacterial suspension, 48 h | 97.1% |
| Ref 47 | 100 % | Seawater, 90 d | Almost no fouling |
| Ref 48 | 97.8% (80 °C) | Bacterial suspension, 24 h | 85.4% |
| Ref 49 | 48.7% (90 °C) | Bacterial suspension, 24 h | 100% |
| Ref 50 | 85% | Bacterial and algal suspension, 7 d | 99.7% |
| Ref 51 | 85% | Bacterial suspension, 7 d | 99.6% |
| Ref 52 | 92.2% | Bacterial suspension, 15 d | 99.4% |

Tab. S4 The original experimental data and the arranged data for Arrhenius fitting.

| $t$ / ℃ | $T$ / $K$ | $\eta$ | $k$ / $s^{-1}$ |
|---|---|---|---|
| 18 | 291.15 | 0.46 | $6.64\times10^{-4}$ |
| 25 | 298.15 | 0.57 | $9.38\times10^{-4}$ |
| 37 | 310.15 | 0.85 | $2.36\times10^{-3}$ |
| 50 | 323.15 | 0.98 | $5.12\times10^{-3}$ |

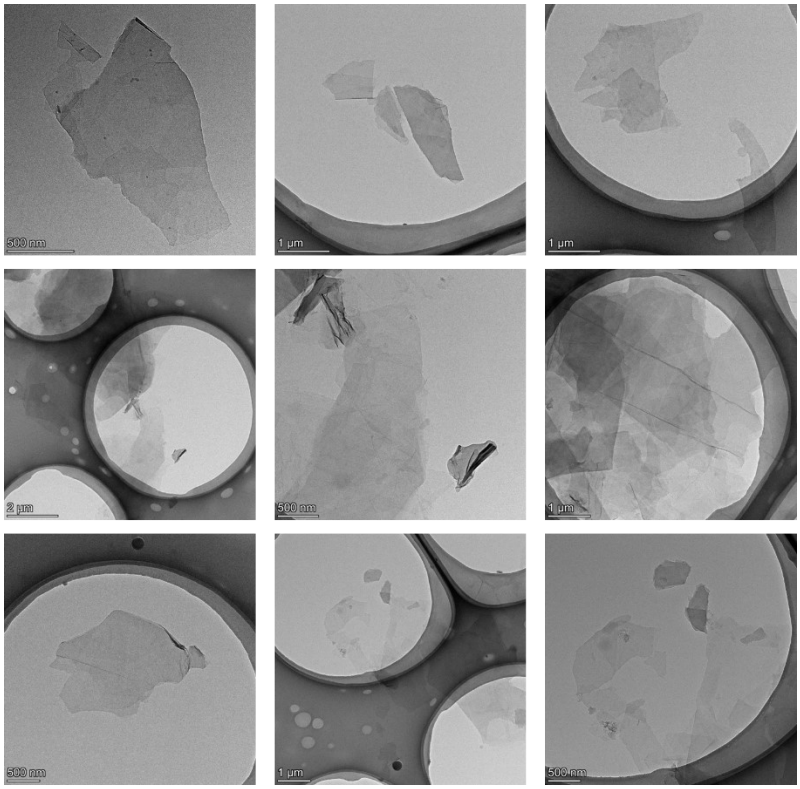

Fig. S1 TEM images of s-GO.

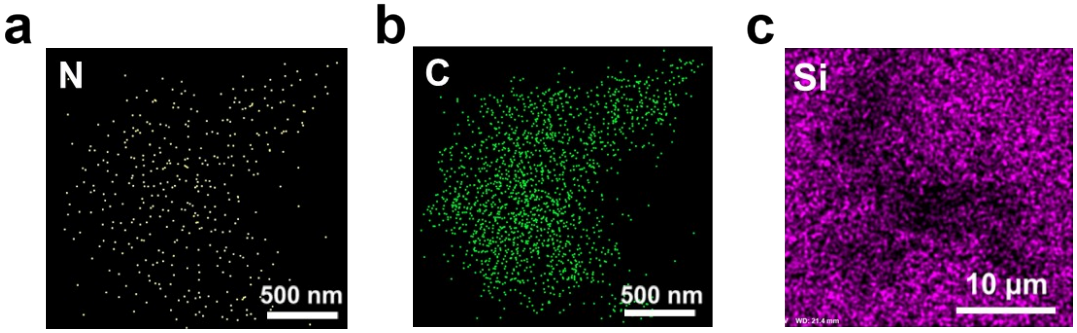


Fig. S2 TEM-EDS mapping of s-GO: (a) N and (b) C. (c) Si in the cross-section of SDC-G characterized by SEM-EDS mapping.

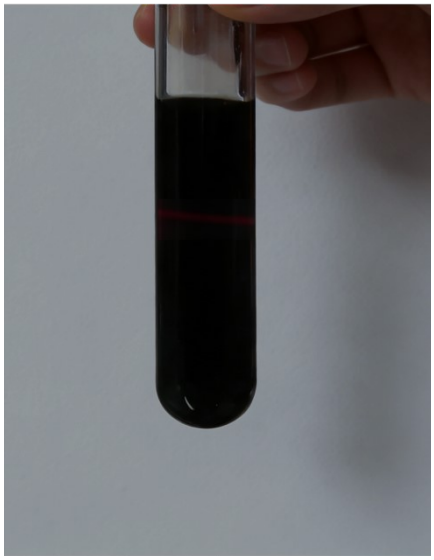

Fig. S3 Photograph of s-GO dispersed in SDC-G prepolymer solution after standing for more than 180 d.

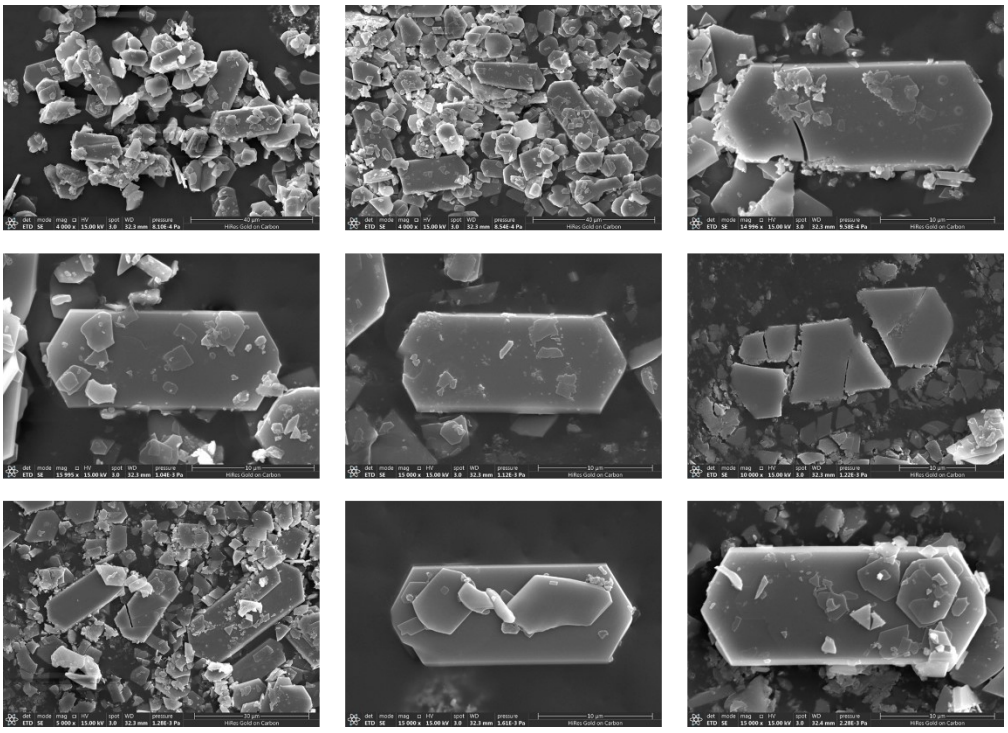

Fig. S4 SEM images of Ag-BTC.

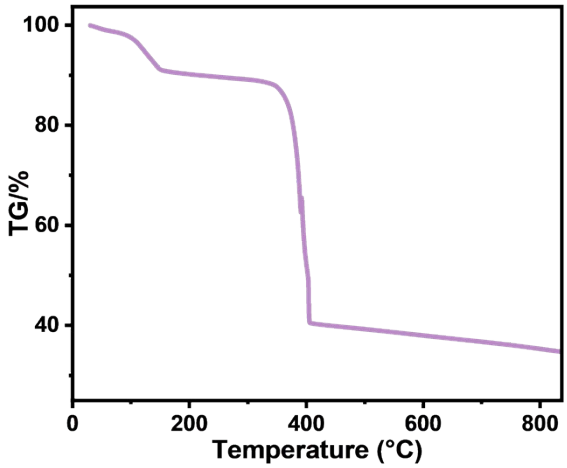


Fig. S5 TG curve of Ag-BTC.

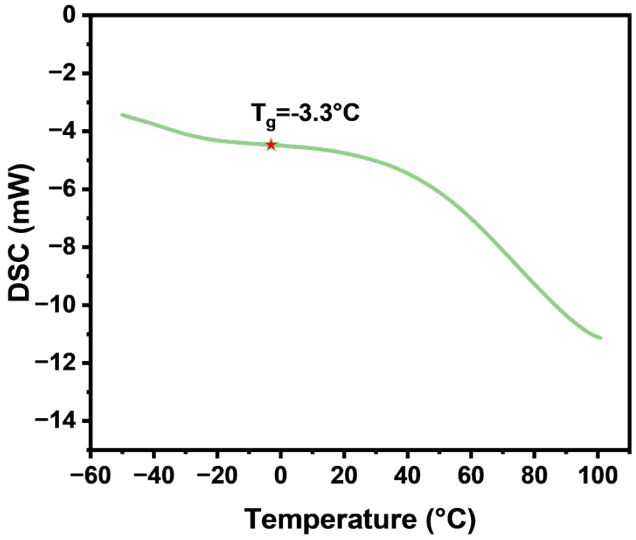


Fig. S6 DSC curve of SDC.

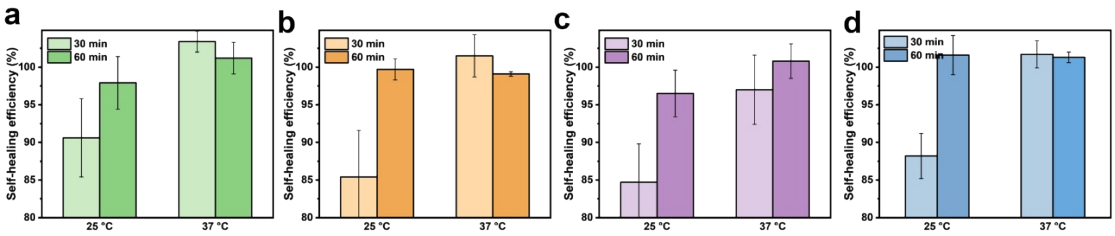


Fig. S7 Self-healing efficiency of (a) SDC, (b) SDC-G, (c) SDC-M and (d) SDC-GM calculated based on the strain recovery ratio.

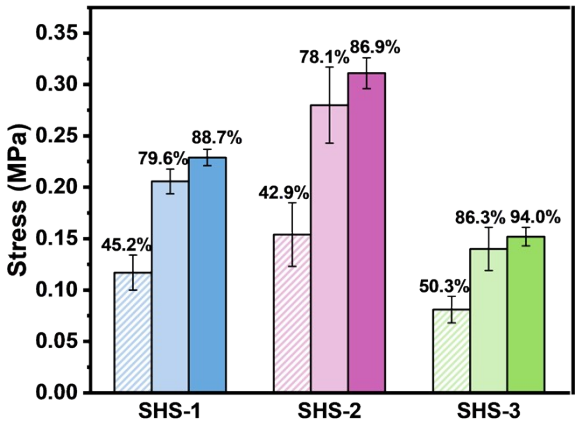


Fig. S8 Tensile strength and self-healing efficiency of SHS. In each group, the data from left to right correspond to 0 h, 24 h, and 216 h after healing.

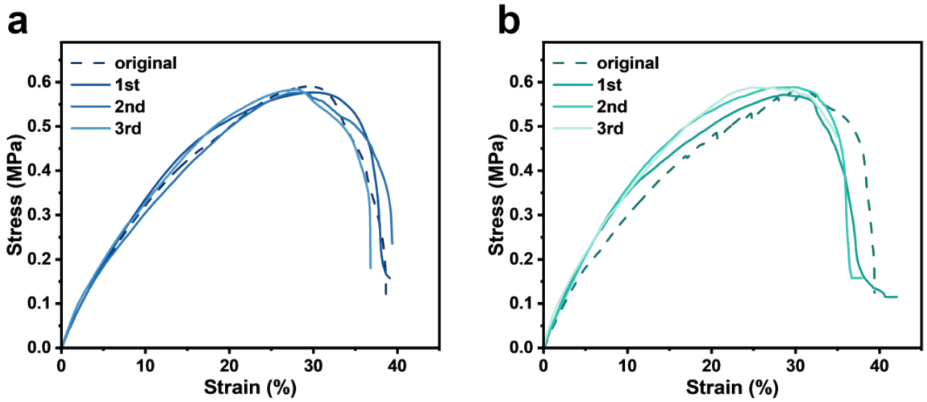


Fig. S9 Stress-strain curves of SDC-GM after 3 cyclic healing at (a) 25 °C and (b) 37 °C.

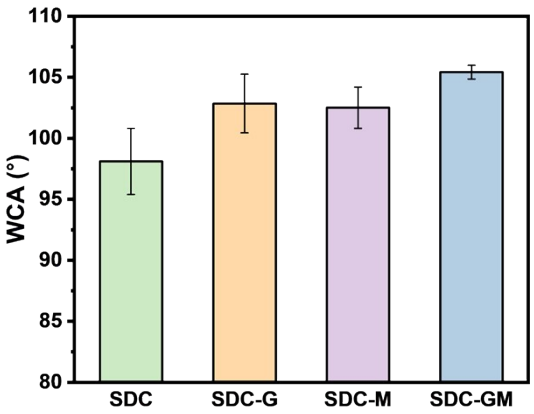


Fig. S10 WCA of SDC, SDC-G, SDC-M, and SDC-GM.

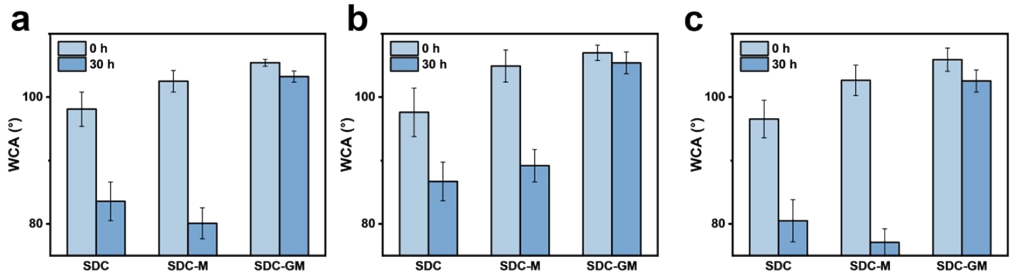


Fig. S11 WCA of SDC, SDC-G, and SDC-GM before and after antifouling test.

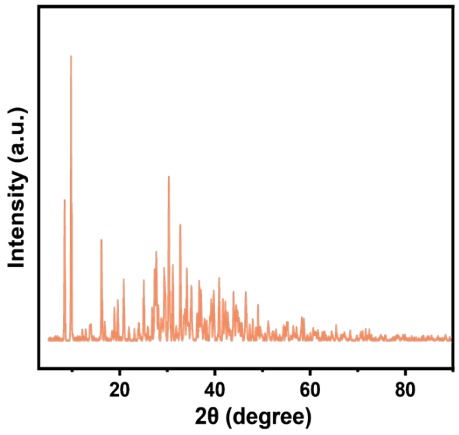


Fig. S12 XRD pattern of Ag-BTC.

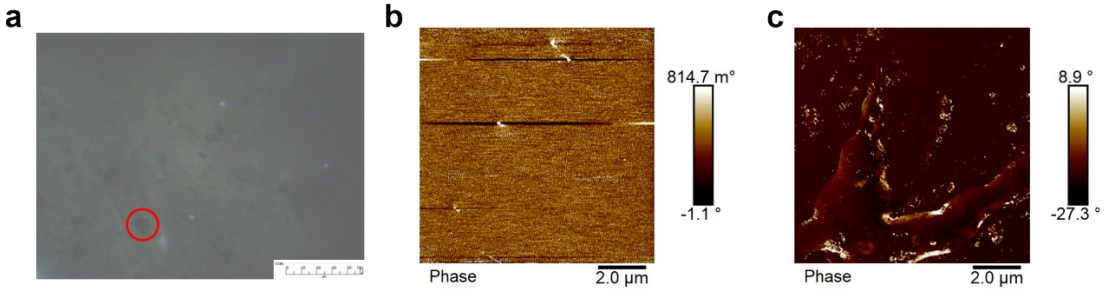


Fig. S13 (a) Optical microscopy image of s-GO dispersion in SDC-G captured simultaneously with the AFM probe. (b) AFM phase image of the region containing s-GO in the cross-section of SDC-G. The s-GO sheets are thin and soft without protruding from the material surface, leading to a flat surface. (c) AFM phase image of the Ag-BTC protrusion in the cross-section of SDC-M.

## References

1. H. Li, T. Ma, Y. Wu, H. Qi, G. Zhang and H. Li, Prog. Org. Coat., 2026, 212, 109894.
2. S. Zhang, Y. Tang, X. Wang, Y. Shen, T. Zhou, C. Lu, F. Guo and W. Shi, Small, 2025.
3. H. Zhao, X. Zang, Y. Shen, M. Tan, P. Wang and J. Wu, ACS Appl. Mater. Interfaces, 2025,

17(17), 25774–25790.
4. C. Liu, C. Ma, Q. Xie and G. Zhang, J. Mater. Chem. A, 2017, 5(30), 15855–15861.
5. Q. Rao, Y. Lu, L. Song, Y. Hou, X. Zhan and Q. Zhang, ACS Appl. Mater. Interfaces, 2021, 13(33), 40032–40041.
6. G. Zeng, S. Chen, Y. Zhou, G. Li, G. Li, J. Zhu, C. Xu and Y. Xin, ACS Appl. Mater. Interfaces, 2025, 17(26), 38532–38544. DOI: 10.1021/acsami.5c08161.
7. Y. Jing, F. Meng, F. Wang and L. Liu, Prog. Org. Coat., 2026, 210, 109645.
8. J. Sun, S. Zhao, C. Song, Y. Zhu, J. Duan, X. Zhai, B. Hou, C. Gao and Y. Liu, Prog. Org. Coat., 2025, 206, 109357.
9. H. Xiao, K. Zhang, T. Gui and S. Zhou, Chem. Eng. J., 2025, 516, 164087.